Theoretical Prediction of the Dense-Plasma Attachment Length in an Orificed Hollow Cathode

Christopher J. Wordingham,* Pierre-Yves C. R. Taunay,* Edgar Y. Choueiri†

Electric Propulsion and Plasma Dynamics Laboratory

Princeton University, Princeton, NJ 08544 USA

The attachment length for a hollow cathode with a narrow, restrictive orifice is computed theoretically without reliance on external models or plasma property data. This critical length controls both the temperature profile and the evaporation-limited life of the cathode emitter; however, no self-consistent model currently exists to calculate the attachment length without experimental data. Charge-exchange-limited ambipolar diffusion is assumed to govern the plasma density evolution in the insert and orifice regions, and the diffusion equation with an electron-impact-ionization source term is solved in one- and two-dimensional forms within the orifice and insert regions respectively. Continuity of the plasma density between the two solutions at the orifice inlet is assumed in order to find an analytical solution using standard partial differential equations techniques. An approximate boundary condition that imposes zero net flux across the plane parallel to the orifice inlet surface is used to calculate the electron temperature in the insert region and the minimum dense-plasma attachment length. This condition allows for the calculation of the two-dimensional variation of the plasma density within the insert region and the electron temperature from first principles in a self-consistent fashion with only neutral density or pressure and heavy particle temperature as model inputs. The plasma density solution and the attachment length obtained by this method for the NSTAR discharge cathode agree well with that observed experimentally and results derived by previous authors.

List of Symbols

Constants		
e	Elementary charge	1.602×10^{-19} C
k_B	Boltzmann's constant	1.38×10^{-23} J/K
m	Electron mass	9.1×10^{-31} kg
Circuit parameters		
I_d	Discharge current	A
R_p	Plasma resistance	Ω
Geometry		
$\bar{r}_o$	Orifice radius normalized to insert radius	
L_i	Insert length	m
L_o	Orifice length	m
R	Cathode (insert) radius	m
r_o	Orifice radius	m
Plasma parameters		
$\bar{n}_e$	Average electron density	m^{-3}
η_p	Plasma resistivity	Ω·m
D_a	Ambipolar diffusion coefficient	m^2/s
J_e	Electron current density	A/m^2
n_e	Electron density	m^{-3}
n_g	Neutral gas density	m^{-3}
n_i	Ion density	m^{-3}
T_{eV}	Electron temperature	V
T_{iV}	Ion temperature	V

*Graduate Research Assistant, EPPDyL; Mechanical and Aerospace Engineering Dept., Student Member AIAA.

†Chief Scientist, EPPDyL; Professor, Applied Physics Group, Mechanical and Aerospace Engineering Dept.; Fellow AIAA.

v_B	Bohm velocity	m/s
Collisions		
λ_{pr}	Energy exchange mean free path	m
ν_{ei}	Electron-ion collision frequency	s
ν_{en}	Electron-neutral collision frequency	s
σ_{CEX}	Charge-exchange cross section	m^2
σ_{en}	Electron-neutral collision cross section	m^2
σ_{iz}	Ionization cross section	m^2
Gas properties		
ϵ_i	Ionization energy	eV
M	Ion or neutral particle mass	kg

I. Introduction

Hollow cathodes for the next generation of Hall and ion thrusters will require increasingly high discharge currents and operational lifetimes. "Near-term" projections for the required discharge powers are in the range of 100 to 200 kW,[1] with some proposed missions demanding operational lifetimes of up to 100 kh.[2,3] For a specific impulse in the 2000 to 6000 s range, this translates to discharge currents of up to 700 A.[4,5] Cathodes operating at lower current have undergone life tests of up to 50 kh,[6] and a cathode capable of providing up to 300 A of discharge current — with an estimated lifetime of 10 to 20 kh — has been developed by Goebel *et al.*.[5] Since life tests are both time-consuming and costly, there is a clear need for the development of models that can accurately estimate the operational life of hollow cathodes. Unfortunately, in order to estimate the evaporation rate of the emitter material we must have an estimate for the area over which the majority of the discharge current is extracted, which depends on both the plasma density profile and the emitter temperature profile.

The length within a hollow cathode over which the internal plasma is sufficiently dense to support temperature-limited (TL) thermionic emission, or where plasma is "attached," not only influences the emitter temperature profile, but also its operational life, and the maximum current that can be extracted from the hollow cathode before the emitter evaporation rate becomes too great. Emission current density is usually axially nonuniform, and may peak sharply near the orifice (especially for high-pressure dispenser cathodes), making prediction of the emitter life substantially more difficult than for vacuum cathodes. The axial plasma density profile also has a pronounced maximum near the orifice for certain cathode operating conditions,[7,8] creating the possibility for space-charge-limited (SCL) emission in the upstream portion of the emitter.

The attachment length has been identified by several terms, including the emission length,[9] active zone,[10] plasma penetration depth,[9] conduction length,[8] or ion production region.[11] These terms are often used interchangeably, but it is not necessarily guaranteed that ion production allows for TL as opposed to SCL emission, or that plasma extends over the entire region of maximum emitter temperature (which typically characterizes the active zone). In addition, early work from the single-channel hollow cathode literature has implied that the dense plasma may extend beyond the active emission area.[10] The typical attachment length or "active zone" for a single-channel cathode is on the order of the tube diameter, and this region can occur upstream from the exit by approximately the tube diameter.[12] No such simple relationship between the cathode geometry and attachment length exists for orificed hollow cathodes. Unfortunately, increasing the pressure or discharge current also tends to decrease the attachment length within an orificed hollow cathode.[8,9] If the pressure is reduced, the attachment length tends to increase, but usually at the cost of higher sheath voltages — and increased exposure to the collisionless plume plasma in the case of very large orifice diameters[8,9] — increasing ion bombardment energies at the emitter surface.

Several approaches to calculate the attachment length have been proposed. 0-D models either include a direct dependency on the energy-exchange mean free path for emitted electrons,[13,14] an ambipolar-diffusion-dominated density decay,[8] empirical correlations of the attachment length as function of the cathode internal pressure,[9] iterative calculations to minimize the power deposited in the sheath,[15] or simply use the attachment length as a free parameter to fit experimental data.[9] One-[16] and two-dimensional models[17] generally require experimental data as input and are more computationally intensive than 0-D or analytical models. Both the pressure-correlation and electron-energy-exchange mean free path methods have drawbacks when applied to new or different cathodes than those for which they were originally developed. The latter model, for instance, vastly underpredicts the length scale over which the plasma density decays when applied to the NSTAR discharge cathode, and the former tends to require parameters outside the range of proposed values to fit experimental data.[18]

We have therefore chosen to revisit the ambipolar-diffusion-dominated density decay from Ref. 8, altering it to provide a self-consistent theoretical framework to estimate the attachment length while minimizing the dependence on experimental data. Our approach combines a 0-D plasma power balance to calculate the average orifice density, a 1-D radial diffusion model to calculate the electron temperature and density profile in the orifice region, and a 2-D diffusion model to calculate the electron temperature and plasma density profile within the insert region. Our approach differs from that presented in Ref. 8 in that it considers appropriate boundary conditions for lower pressure cathodes , features a continuous density profile between the orifice and insert region, and uses a complete orthonormal basis to represent the solution of the ambipolar diffusion equation.

In Section II we discuss the overarching assumptions of our model, and in Sections III and IV, we present the calculations of the electron temperature and density profiles for the orifice and insert regions, respectively. We show a direct comparison of our solution to previous model results and experimental data for both the plasma density profile and the attachment length (axial decay) in Section V.

II. Model Assumptions

The fundamental assumptions required for the analytical solution of the proposed model are the following:

- The plasma density in the insert region is governed by resonant-charge-exchange-limited ambipolar diffusion.
- The Bohm and ambipolar diffusion fluxes are equal at the plasma-sheath boundary, and the Bohm velocity does not depend on the emission current.
- The neutral pressure and heavy particle temperature is constant in each of the model regions.
- The electron temperature in each region is spatially uniform and constant.
- The orifice plasma density is assumed not to vary in the axial direction.
- The plasma density is continuous across the orifice/insert boundary, and we assume that the plasma density along the orifice plate decays exponentially in the radial direction.
- The net flux across the plane parallel to the orifice plate surface in the insert region is zero.

Our first assumption is generally justified given that the cross section for resonant charge exchange in typical inert gases is very large[8,19,20] and $\mu_e \gg \mu_i$. The second assumption allows for an improvement over previous model boundary conditions (e.g., those used in Refs. 8,16) in that the plasma density is not assumed to be zero at the "wall" or, more accurately, the plasma-sheath boundary. This improved, more-general boundary condition used in this model is well known in other plasma modeling approaches.[21] Asserting that $n_e \to 0$ at the boundary overestimates the diffusion losses to the walls and therefore overpredicts the required electron temperature for a given cathode pressure and geometry. Taking the Bohm velocity to be constant greatly simplifies the dependence of the boundary conditions for the insert plasma model on operating conditions. This assumption has been used in most, if not all, previous cathode models and is also a reasonable approximation in general as the energy of ions entering the sheath does not typically vary by more than 20% of the value for a non-emitting wall.[22]

Measurements of the heavy particle temperature have not been performed in the insert or orifice regions, so it is difficult to determine how well we can approximate the neutral or ion temperatures as constants in either region. However, this assumption is also generally common to all but 2-D computational models. According to Poiseuille flow models,[8,23] we would be justified in approximating the pressure in the insert region as a constant (as is done in Refs. 8,13,16,24), but these models are not strictly applicable for cathode conditions and fail to incorporate the two-dimensional effects near the orifice constriction. Strong pressure gradients are likely to exist in the orifice, but we assume constant pressure in this region and use the average pressure in order to make the solution tractable. The assumption that the orifice plasma density is axially uniform is likely to be equally unjustified, but we wish to focus on the density decay in the insert region. We therefore use a one-dimensional radial solution in the orifice to capture the effect of the orifice size and radial density distribution without making the solution exceedingly complex.

Our final two assumptions are unique to this model and are used to couple the insert and orifice solutions and to calculate the insert electron temperature assuming the radially-averaged maximum insert plasma

density occurs at the orifice inlet surface, respectively. The latter is not well-justified theoretically, as we would prefer to impose the Bohm flux along the orifice plate surface and a separate flux along the orifice inlet, but this has proven to be exceptionally difficult. Rather than complicate the analytical solution further, and in the absence of a good model for the flux into the insert region from the orifice, we chose to impose the zero flux condition in order to bound the attachment length to its likely minimum value. In addition to bounding the minimum value of the attachment length, the final assumption also gives us an independent expression with which to self-consistently solve for the insert electron temperature without relying on the solution for the lowest-order eigenvalue as in Ref. 8. The assumption of a given, strictly positive functional form for the density decay away from the orifice in the radial direction is necessary to extend the Dirichlet information along the entire insert region downstream boundary. If we were not to make this assumption, an analytical solution by standard partial differential equation techniques would not be possible.

III. One-Dimensional Radial Diffusion Model

In order to avoid unnecessary complexity in our solution, we treat the orifice plasma as axially uniform and model only the radial variation. This level of fidelity is important as the orifice solution is later included as a boundary condition for the insert solution, but taking the extra step toward a full 2-D model of the orifice would require boundary information beyond what can be obtained from a power balance. The steady-state density in a cylindrical geometry can be found from the time-independent ambipolar diffusion equation:

$$\frac{d^2 n_e}{dr^2} + \frac{1}{r}\frac{dn_e}{dr} + \frac{\nu_{iz}}{D_a} n_e = 0. \tag{1}$$

Equation 1 may be written in terms of a normalized radius:

$$\frac{d^2 n_e}{d\bar{r}^2} + \frac{1}{\bar{r}}\frac{dn_e}{d\bar{r}} + \gamma^2 n_e = 0, \tag{2}$$

where $\bar{r} = r/R$ and

$$\gamma^2 = R^2 \frac{n_g \sigma_{iz} \bar{v}}{D_a}. \tag{3}$$

A. General solution

Equation 2 is a Helmholtz equation with unknown γ. In radial coordinates with $\bar{r} \in [0, 1]$ its bounded solution is a zeroth-order Bessel function of the first kind,

$$n_e = C J_0 \left(\gamma \bar{r}\right), \tag{4}$$

where C is a proportionality constant.

Previous authors[8] have used a homogeneous Dirichlet boundary condition at the wall ($n_e\left(\bar{r} = 1\right) = 0$). This boundary condition is valid for high-pressure discharges[21] such as the ones encountered in the NSTAR neutralizer cathode[8] or cathodes with small orifice-to-insert diameter ratios.[23] A Robin boundary condition is more appropriate in the context of hollow cathodes, where the insert and orifice pressures are typically within the range of 1 to 10 Torr. The Robin boundary condition enforces continuity at the plasma-sheath boundary and equates the Bohm and diffusion fluxes:

$$-D_a \frac{dn_e}{dr} = n_e v_B \Leftrightarrow \frac{dn_e}{d\bar{r}} + n_e \delta = 0, \tag{5}$$

where $\delta = v_B R/D_a$ and can be interpreted as a measure of the ratio of the Bohm velocity to the average radial diffusion velocity.

Each type of boundary condition generates an infinite set of positive and increasing eigenvalues. The Dirichlet boundary condition requires γ to be a zero of J_0, while the Robin boundary condition yields the following transcendental equation for γ:

$$-\gamma J_1\left(\gamma\right) + \delta J_0\left(\gamma\right) = 0. \tag{6}$$

Since we do not have inhomogeneous Dirichlet information along any boundary of the orifice and assumed our solution was one-dimensional, we retain only the first eigenmode for the solution — retaining further

terms would render the coefficients of the eigenmodes impossible to determine. This allows us to compute the maximum electron temperature for the orifice region with Eq. 3 and the smallest eigenvalue found using Eq. 6. The same procedure can also be used to determine the maximum permissible electron temperature in the insert region, though we do not use this value as the model electron temperature as we do in the orifice solution.

We also observe that the electron temperature and therefore density profile in the proposed model depends only on the product of the neutral density and radius of the region of interest. If we have a fixed value of the heavy particle temperature, we can calculate the electron temperature for both types of boundary condition in terms of the pressure-diameter product, as shown in Figure 1. This also demonstrates that the two boundary conditions yield identical solutions in the limit of high pressure. Above $P_g d = 1$ Torr-cm the two solutions for T_{eV} differ by less than 5%. We shall assume the more general case of the Robin boundary condition for the remainder of this paper, as the Dirichlet condition is likely to become problematic for some cathode orifice pressures.

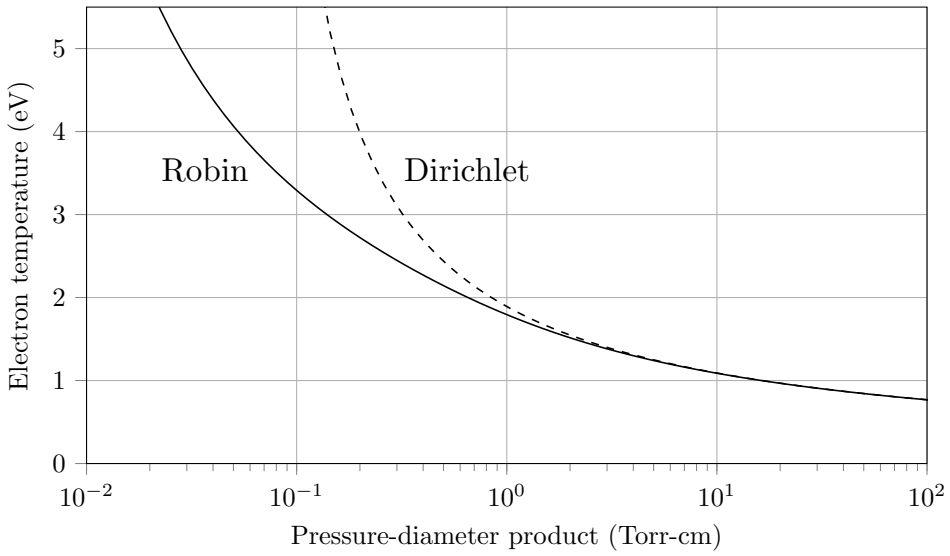

Figure 1. Dependence of electron temperature on the pressure-diameter product expressed in Torr-cm for both forms of radial boundary condition with T_i fixed at 3000 K.

B. Orifice

For the single-eigenmode orifice solution, the proportionality constant in Eq. 4 corresponds to the maximum density in the orifice, n_{or}, which is computed from the average density:

$$\bar{n}_e = \frac{\int_0^{\bar{r}_o} n_{or} J_0(\gamma s)\, s\, \mathrm{d}s}{\pi \bar{r}_o^2} \Leftrightarrow n_{or} = \frac{\gamma \bar{r}_o}{2 J_1(\gamma \bar{r}_o)} \bar{n}_e \tag{7}$$

The average density is determined using the power balance from Ref. 8:

$$R_p I_d^2 = \frac{5}{2} I_d \left(T_{eV} - T_{eV}^{\mathrm{ins}}\right) + n_g \bar{n}_e e \langle \sigma_{iz} v_e \rangle \epsilon_i \left(\pi r_o^2 L_o\right), \tag{8}$$

where R_p is the plasma resistance, I_d the total cathode discharge current, T_{eV} the electron temperature, n_g the neutral density in the orifice, σ_{iz} the cross-section for electron-impact ionization, and ϵ_i the total ionization energy. The plasma resistance is calculated with the plasma resistivity and orifice geometry:

$$R_p = \eta_p \frac{L_o}{\pi r_o^2}. \tag{9}$$

The resistivity is computed based on the electron-ion and electron-neutral collision frequencies and the average electron density (because the exact distribution of the current density within the orifice plasma is

unknown):

$$\eta_p = \frac{m}{\bar{n}_e e^2}\left(\nu_{ei} + \nu_{en}\right). \tag{10}$$

The electron-ion collision frequency is calculated using:

$$\nu_{ei} = 2.9 \times 10^{-12} \bar{n}_e \frac{\ln \Lambda}{T_{eV}^{3/2}}. \tag{11}$$

Both the electron-neutral and ionization reaction rates rely on Maxwellian-averaged cross sections calculated using Hayashi's most recent data (Ref. 25). The Coulomb logarithm is given by:

$$\ln \Lambda = 23.0 - \frac{1}{2}\ln\left(10^{-6}\bar{n}_e T_{eV}^{-3}\right). \tag{12}$$

IV. Insert Region Diffusion Model

We consider the two-dimensional, axisymmetric diffusion equation with a source term corresponding to volumetric ionization to compute the steady-state plasma density in the insert region. Using normalized coordinates $\bar{r} = r/R$ and $\bar{z} = z/R$, this equation may be written as:

$$\frac{\partial^2 n_e}{\partial \bar{r}^2} + \frac{1}{\bar{r}}\frac{\partial n_e}{\partial \bar{r}} + \frac{\partial^2 n_e}{\partial \bar{z}^2} + \gamma^2 n_e = 0, \tag{13}$$

where

$$\gamma^2 = R^2 \frac{n_g \sigma_{iz} \bar{v}}{D_a}. \tag{14}$$

The value of γ is found using the value of T_{eV} from the flux condition at the orifice plate discussed in the following section.

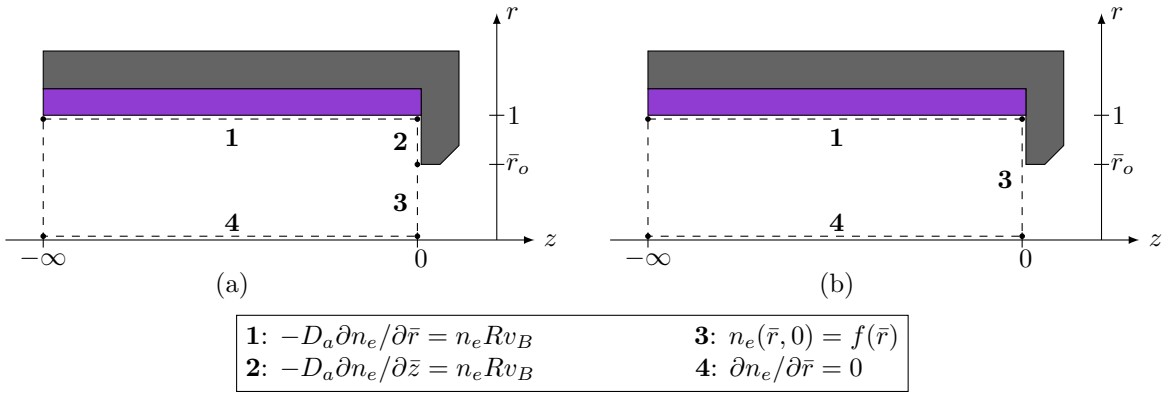

Figure 2. Mathematical representation of the insert region for two different cases: (a) General case with non-linear boundary condition at $z = 0$ and (b) Infinite-length insert with linear boundary condition.

A. Boundary conditions

The insert region is axisymmetric with a Robin boundary condition at the insert surface (Eq. 5) and a homogeneous Neumann boundary condition on the centerline to enforce symmetry about the cathode axis. In the axial direction, the extent of the solution domain is assumed to be infinite, so the solution must be bounded as $\bar{z} \to -\infty$ upstream of the orifice. Different sets of boundary conditions at $\bar{z} = 0$ may be used to represent the boundary value problem, with two cases shown in Fig. 2. The most general representation (Fig. 2 (a)) includes an additional Robin boundary condition on the orifice plate surface and a Dirichlet condition enforcing continuity with the orifice solution along the orifice inlet. This piecewise boundary condition prevents the use of standard partial differential equation techniques such as separation of variables and requires numerical techniques. To obtain an analytical solution, we propose a simplification of the boundary condition on the orifice plate, as shown in Fig. 2 (b).

The boundary condition for $\bar{z} = 0$ and $\bar{r} \in [0, \bar{r}_o]$ is represented by the orifice solution. This solution is extended for $\bar{r} \geq \bar{r}_o$ by imposing three constraints:

1. The extension is C^0 at $\bar{r} = \bar{r}_o$.
2. The extension is C^1 at $\bar{r} = \bar{r}_o$.
3. The extension verifies the boundary condition imposed at $\bar{r} = 1$.

These three constraints can be used with any functional representation of the density which features up to three parameters. The first two conditions ensure that the density and the flux are continuous at the orifice edge, and the third constraint ensures that the extended function can be represented by the solutions of the eigenvalue problem. The functional representation should also be positive for $\bar{r} \geq \bar{r}_o$.

We propose the use of an exponential decay to satisfy all requirements. The density at $\bar{z} = 0$ is represented by:

$$\begin{cases} n_{or} J_0 \left(\gamma_{or} \bar{r}\right), \, \bar{r} \leq \bar{r}_o \\ x_0 \exp\left(x_1 \bar{r}\right) + x_2, \, \bar{r} \geq \bar{r}_o \end{cases}, \tag{15}$$

where the subscript *or* denotes orifice quantities. The imposed constraints form a non-linear system for the continuation function coefficients. We give the case for the Robin boundary condition below:

$$\begin{cases} x_0 \exp\left(x_1 \bar{r}_o\right) + x_2 - J_0\left(\gamma_{or} \bar{r}_o\right) = 0 \, (C^0) \\ x_0 x_1 \exp\left(x_1 \bar{r}_o\right) + \gamma_{or} J_1\left(\gamma_{or} \bar{r}_o\right) = 0 \, (C^1) \\ x_0 x_1 \exp\left(x_1\right) + \delta \left(x_0 \exp\left(x_1\right) + x_2\right) = 0 \, (\text{Robin}) \end{cases} \tag{16}$$

The non-linear system is solved using the Newton-Krylov solver implemented in the Scipy library.[26] It can be shown that for this particular choice of the continuation function, the system of coefficient expressions can be reduced to a single non-linear equation for one of the coefficients, which can then be back-substituted to obtain the remaining values, but the Newton-Krylov solution method is general and can be applied to any choice of continuation function.

In order to self-consistently obtain the electron temperature, we cannot use the temperature from the single-eigenmode approximation as in previous insert models.[8] Therefore, in order to both obtain the electron temperature and restrict our focus to the *minimum* attachment length, we impose the condition that the total net flux to/from the orifice and orifice plate must be zero. Viewed from a 1-D axial perspective, this ensures that the maximum radially averaged density occurs at the orifice, yielding strictly decaying solutions. The solution of Eq. 13 obtained with this approach should satisfy flux conditions on both the orifice plate and orifice hole at $\bar{z} = 0$:

$$\begin{cases} \Phi_{or} = 2\pi R \displaystyle\int_0^{\bar{r}_o} \left(-D_a \frac{\partial n_e}{\partial \bar{z}}\right) s \, \mathrm{d}s \leq 0, \text{ for } \bar{r} \leq \bar{r}_o \\ \Phi_{pl} = 2\pi R \displaystyle\int_{\bar{r}_o}^{1} \left(-D_a \frac{\partial n_e}{\partial \bar{z}}\right) s \, \mathrm{d}s \geq 0, \text{ for } \bar{r}_o \leq \bar{r} \leq 1 \\ \Phi_{pl} + \Phi_{or} = 0 \end{cases} \tag{17}$$

The first two expressions must be checked to ensure that the choice of continuation function can generate a solution for which the fluxes take physically justified directions. $\Phi_{pl} < 0$, for instance, would imply that ions were entering the insert region *from* the orifice plate.

B. Analytical solution

Using the choice of boundary conditions represented in case (b) in Fig. 2 and described above, we solve Eq. 13 using separation of variables:

$$n_e = R\left(\bar{r}\right) Z\left(\bar{z}\right).$$

The Robin boundary condition at $\bar{r} = 1$ gives a condition on the eigenvalues of the problem, and the application of both the inhomogeneous Dirichlet boundary condition at $\bar{z} = 0$ and $n_e \to 0$ as $\bar{z} \to -\infty$ allow for the computation of the unknown coefficients for the solution.

EIGENFUNCTIONS We obtain the solution for each eigenmode,

$$\phi_k = C_k J_0\left(\lambda_k \bar{r}\right) \exp\left(\alpha_k \bar{z}\right), \tag{18}$$

where α_k is the separation constant, $\lambda_k^2 = \gamma^2 + \alpha_k^2$, and C_k is the coefficient for each eigenmode. The separation constant is strictly positive, as other cases yield non-vanishing densities for $\bar{z} \to -\infty$.

SEPARATION CONSTANT The boundary condition at $\bar{r} = 1$ yields the eigenvalues λ_k and therefore the corresponding separation constant α_k. In the case of a Robin boundary condition, the λ_k verify the transcendental equation

$$\frac{D_a \lambda_k J_1\left(\lambda_k\right)}{R} = v_B J_0\left(\lambda_k\right) \Leftrightarrow \lambda_k J_1\left(\lambda_k\right) = \delta J_0\left(\lambda_k\right), \tag{19}$$

where $\delta = v_B R / D_a$. Equation 19 yields an infinite number of increasing and unique eigenvalues. The superposition of all eigenmodes gives the solution of the diffusion equation:

$$n_e\left(\bar{r}, \bar{z}\right) = \sum_{k=1}^{+\infty} C_k J_0\left(\lambda_k \bar{r}\right) \exp\left(\alpha_k \bar{z}\right) \tag{20}$$

EIGENMODE COEFFICIENTS The constants C_k are determined with the Dirichlet boundary condition at $\bar{z} = 0$ and the orthogonal properties of the Bessel functions:

$$\sum_{k=1}^{+\infty} C_k J_0\left(\lambda_k \bar{r}\right) = \begin{cases} n_{or} J_0\left(\gamma_{or} \bar{r}\right), \, \bar{r} \leq \bar{r}_o \\ f_c(\bar{r}), \, \bar{r} \geq \bar{r}_o \end{cases}, \tag{21}$$

where $f_c(s)$ is the continuation function. Multiplying Equation 21 by $\bar{r} J_0\left(\lambda_m \bar{r}\right)$ and integrating for $\bar{r} \in [0, 1]$ yields:

$$C_m = \frac{1}{\int_0^1 s J_0\left(\lambda_m s\right)^2 \, \mathrm{d}s} \cdot \left(\int_0^{\bar{r}_o} s n_{or} J_0\left(\gamma_{or} s\right) J_0\left(\lambda_m s\right) \, \mathrm{d}s + \int_{\bar{r}_o}^1 s f_c\left(s\right) J_0\left(\lambda_m s\right) \, \mathrm{d}s \right) \tag{22}$$

The integration may be carried out analytically excluding the integral involving the continuation function:

$$C_m = \frac{2}{\left(J_0^2\left(\lambda_m\right) + J_1^2\left(\lambda_m\right)\right)} \cdot \left[\frac{n_{or} \bar{r}_o}{\gamma_{or}^2 - \lambda_m^2} \left(\gamma_{or} J_0\left(\lambda_m \bar{r}_o\right) J_1\left(\gamma_{or} \bar{r}_o\right) - \lambda_m J_0\left(\gamma_{or} \bar{r}_o\right) J_1\left(\lambda_m \bar{r}_o\right) \right) + \ldots \right.$$
$$\left. \int_{\bar{r}_o}^1 s f_c\left(s\right) J_0\left(\lambda_m s\right) \, \mathrm{d}s \right]. \tag{23}$$

The remaining integral is calculated numerically.

C. Insert electron temperature

As mentioned earlier, we use the electron temperature which balances the total particle flux from the orifice, Φ_{or}, with the total flux to the orifice plate, Φ_{pl}. This assumption is equivalent to the assertion that the maximum radially averaged density is obtained at the orifice, consistent with our representation of the solution. The decaying solutions obtained represent the minimum attachment length (assuming that the net flux of ions across the orifice inlet is into the insert region), as the solution cannot capture a density maximum at any location other than the orifice inlet. This likely restricts the applicability of our solution to cathodes with narrow orifices, but this assumption was already required by the orifice density solution. In order to find the full solution, we must therefore calculate the solution for an arbitrary T_{eV}, then iterate until the flux boundary condition is met.

D. Algorithm

For a given electron temperature and the required model inputs of pressure and heavy particle temperature in each region, the diffusion equation is solved using the following algorithm:

1. The electron temperature for the orifice is calculated from the first eigenmode of the 1-D radial diffusion problem (Eq. 6).

2. The average and peak densities in the orifice are determined with Eqs. 7 and 8, respectively, and the continuation function is also generated.

3. The insert electron temperature is used to calculate the ambipolar diffusion coefficient and Bohm velocity (or δ) as well as γ for the insert region plasma.

4. The eigenvalues for the insert problem are computed using Eq. 19.

5. The coefficients of each eigenmode are calculated using Eq. 23.

6. The semi-infinite sum of eigenfunctions is computed with a truncated sum, since the $C_m \to 0$ as $m \to \infty$.

7. The orifice and orifice plate fluxes are calculated to determine whether the choice of electron temperature satisfies the boundary condition at $\bar{z} = 0$.

8. If the solution does not satisfy the boundary condition in step 7, the procedure is repeated until the correct electron temperature is found using a bisection algorithm.

V. Results and discussion

We compare the results of our approach to the density measurements along the cathode main axis from Ref. 27 and with the methodology outlined in Ref. 8. We use neutral gas pressures of 4.5 and 7.8 Torr in the orifice and insert regions, respectively, and a heavy particle temperature of 3000 K in both regions. The values were chosen to coincide with the model inputs used for Ref. 8.

A. Verification

First, we verify that the coefficients calculated from Eq. 23 decay as λ_m increases with m. Figure 3 shows the evolution of the eigen-coefficients with increasing m, for $m \leq 50$. The solution we propose features multiple prominent eigenmodes, though most of them decay rapidly. It is important that we have used the sum over multiple eigenmodes, as we can see that the fundamental eigenmode does not necessarily have the largest coefficient due to the constricted shape of the orifice solution compared to the fundamental mode in the insert region. In addition, a single-eigenmode solution in the insert region clearly cannot meet the boundary conditions imposed by the presence of the orifice.

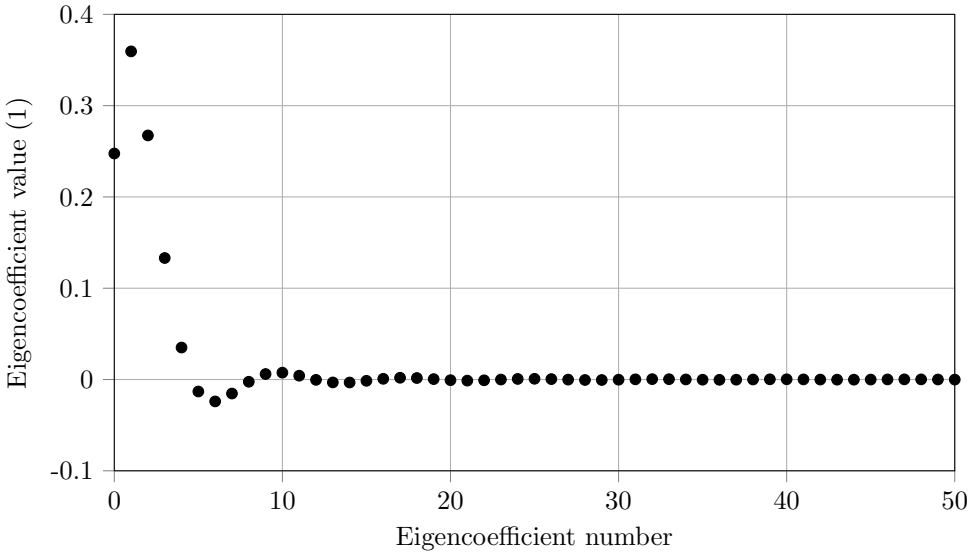

Figure 3. Eigencoefficients C_k.

We verify also that the solution on the orifice follows the imposed Dirichlet boundary condition. Figure 4 shows the normalized density as a function of normalized radius at $\bar{z} = 0$, along with the imposed Dirichlet

boundary condition. We have excellent agreement with the imposed condition from Eq. 15, and we observe that the proposed extension is indeed C^0 and C^1 at $\bar{r} = \bar{r}_o$. Imposing the Robin condition at $\bar{r} = 1$ results in a small, yet non-zero, derivative at that point, as opposed to the solution for the homogeneous Dirichlet condition for which a strong density gradient is expected at the walls. Another important side-effect of the use of the Robin condition is that the plasma density at the sheath edge is readily calculated from the solution, which is necessary for accurately calculating the fluxes to the insert. The Dirichlet condition, on the other hand, artificially increases the flux to the wall for all but very high pressures and makes the calculation of the density at the sheath edge problematic (as an infinite velocity is required for finite flux at zero density).

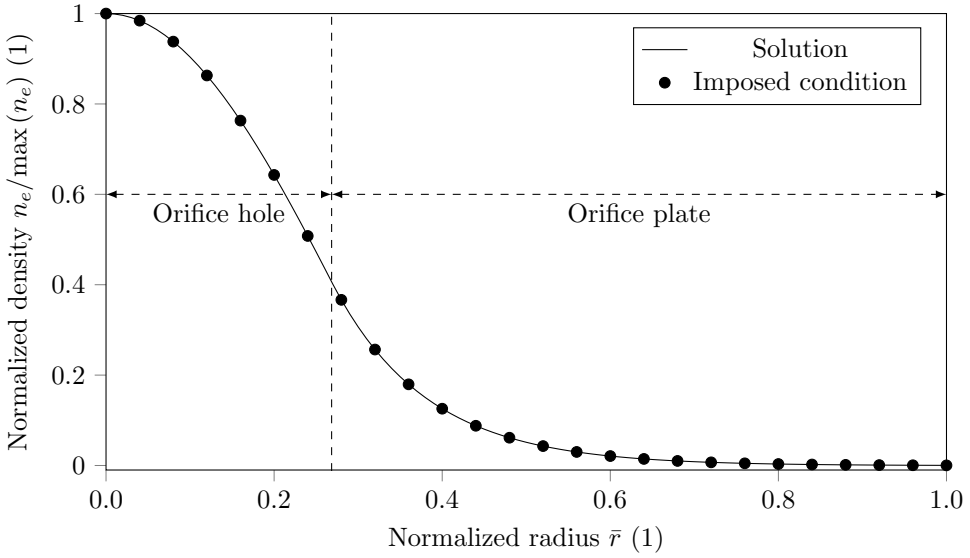

Figure 4. Verification of the imposed Dirichlet boundary condition.

B. Sensitivity analysis

Because the only required model inputs are the neutral densities and heavy particle temperatures in each region (excluding the cathode geometry), and the pressures are generally determined using measurements or flow models, we must determine the sensitivity of the solution to the ion temperature (as it is essentially arbitrary). The variation in the solution result for different heavy particle temperatures is shown in Figure 5. The shape of the solution remains relatively constant when the ion temperature varies by ± 1000 K from the nominal value of 3,000 K, though the resulting electron temperature varies by about $\pm 10\%$.

C. Density profile

Our 2-D model allows for the computation of the plasma density on the entire domain. Figure 6 shows a contour plot of the density calculated for the NSTAR cathode, with an insert pressure of 7.8 Torr and a discharge current of 15 A. The contour features qualitative agreement with previous numerical results for various cathodes and operating regimes as described in Refs. 7, 16, 28–30.

We compare the density calculated using our model along the cathode axis to experimental data and to the results obtained by the method outlined in Ref. 8 in Figure 5. Our model accurately predicts the density decay rate but is not able to capture the increase in density upstream of orifice due to the chosen boundary conditions. The results of the model match that of Ref. 8 but underpredict the experimental plasma density. The most important difference between the two model curves shown is that our calculation only requires the pressures and heavy particle temperatures as inputs, whereas the existing model required that the ion current generated within the insert region be known, which was found using the results of a separate 2-D model which also required further experimental data as input.

Two further insights can be extracted from the new model. First, given that the operator and boundary conditions do not depend on the discharge current with the exception of the scaling of the orifice peak density,

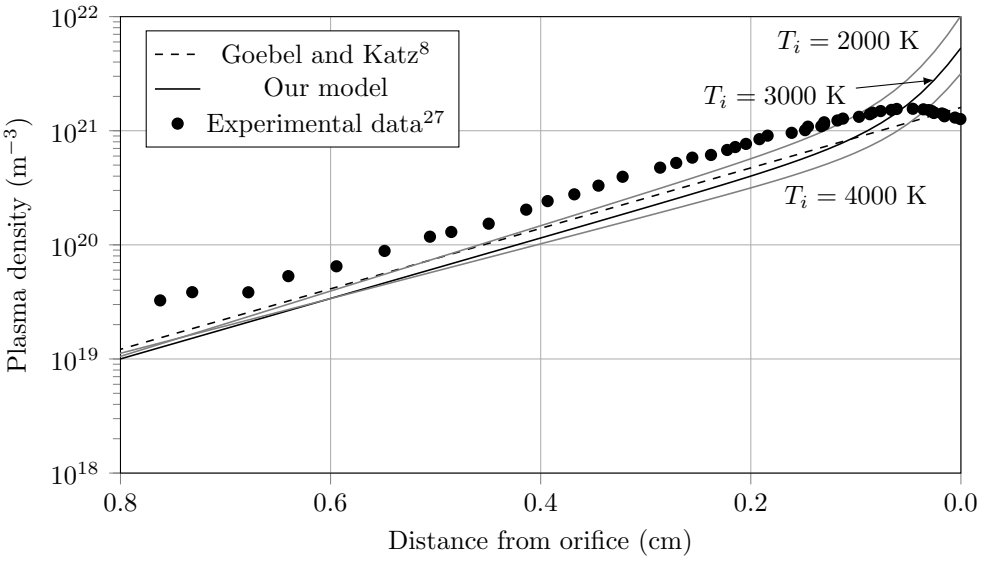

Figure 5. Density decay of the model for varying ion temperature (2000 to 4000 K), and comparison to previous modeling and experimental results for the NSTAR discharge cathode operating at $I_d = 15$ A.

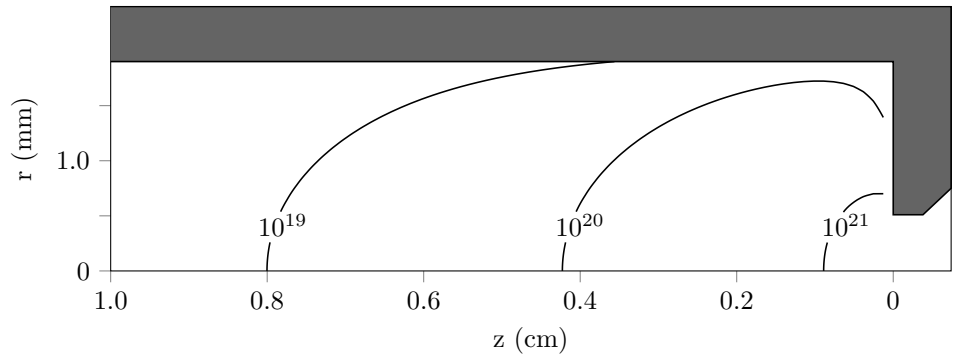

Figure 6. Plasma density contour (m^{-3}) for the NSTAR cathode operating at $I_d = 15$ A.

a theoretical model of this form cannot properly capture the experimentally observed trend of decreasing attachment length with increasing discharge current. The only apparent remediations for this drawback would be to include the dependence of the insert region neutral pressure on the discharge current or to allow the Bohm velocity at the insert boundary to be modified by the emission current density. Second, as mentioned in Section III above for the 1-D solution, the entire operator for the 2-D solution can be shown to depend only on the pressure-diameter product (including the exponential extension) with an additional dependence on the discharge current through the peak density of the orifice model.

VI. Conclusion

We have developed a methodology to analytically determine the decay length of the plasma density within the hollow cathode insert region, using only gas pressures and temperatures as model inputs. The method relies on a charge-exchange-dominated ambipolar diffusion model, and we solve the diffusion equation using one- and two- dimensional approaches for the orifice and insert regions, respectively. We enforce both continuity between the orifice and insert densities as well as a condition of zero net flux along the plane of the orifice plate surface in the insert region, using an exponential continuation of the boundary data in order to allow for a separation solution to the governing PDE. The insert electron temperature is also calculated using the net flux condition imposed across the plane parallel to the orifice inlet, which corresponds to a

condition for the minimum dense-plasma attachment length.

As opposed to previous models, our approach does not rely on external computational models, phenomenological assumptions, correlations with experimental data, or the input of plasma property data from experimental results. The plasma density solution calculated for the NSTAR discharge cathode features qualitative agreement with previous numerical solutions and good agreement with experimental data. The solution within the insert region is self-consistent and is relatively insensitive to the ion temperature parameter.

The most important consequence of this model is that 2-D plasma data including the attachment length (or density decay length scale) and sheath-edge fluxes can be calculated theoretically with pressure and temperature information typically available using 0-D models. The current model iteration applies predominantly to cathodes with restrictive orifices, but work is underway to extend the region of validity of the model.

References

[1]Brown, D. L., et al., "Air Force Research Laboratory High Power Electric Propulsion Technology Development," *IEEE Aerospace Conference*, 2009.

[2]Goebel, D. M. and Chu, E., "High Current Lanthanum Hexaboride Hollow Cathodes for High Power Hall Thrusters," *32nd International Electric Propulsion Conference*, 2011.

[3]Hofer, R.R., et al., "Evaluation of a 4.5 kW Commercial Hall Thruster System for NASA Science Missions," *42nd AIAA/ASME/SAE/ASEE Joint Propulsion Conference & Exhibit*, 2006.

[4]Plasek, M. L., et al., "Experimental Investigation of a Large-Diameter Cathode," *50th AIAA/ASME/SAE/ASEE Joint Propulsion Conference & Exhibit*, 2014.

[5]Goebel, D. M. and Chu, E., "High-Current Lanthanum Hexaboride Hollow Cathode for High-Power Hall Thrusters," *Journal of Propulsion and Power*, 2014.

[6]Shastry, R., et al., "Status of NASAs Evolutionary Xenon Thruster (NEXT) Long-Duration Test as of 50,000 h and 900 kg Throughput," *33rd International Electric Propulsion Conference*, 2013.

[7]Katz, I., et al., "Insert Heating and Ignition in Inert-Gas Hollow Cathodes," *IEEE Transactions on Plasma Science*, 2008.

[8]Goebel, D. and Katz, I., *Fundamentals of Electric Propulsion: Ion and Hall Thrusters*, John Wiley & Sons, Inc., 2008.

[9]Albertoni, R., Pedrini, D., Paganucci, F., and Andrenucci, M., "A Reduced-Order Model for Thermionic Hollow Cathodes," *IEEE Transactions on Plasma Science*, Vol. 41, No. 7, 2013, pp. 1731–1745.

[10]Lorente-Arcas, A., "A Model for the Hollow Cathode Discharge," *Plasma Physics*, Vol. 14, 1972.

[11]Siegfried, D. E., *A Phenomenological Model for Orificed Hollow Cathodes*, Ph.d., Colorado State University, 1982.

[12]Krishnan, M., Jahn, R. G., von Jaskowsky, W. F., and Clark, K. E., "Physical processes in hollow cathode discharge," *AIAA Journal*, Vol. 15, No. 9, 1977, pp. 1217–1223.

[13]Siegfried, D. E. and Wilbur, P. J., "A model for mercury orificed hollow cathodes-Theory and experiment," *AIAA journal*, Vol. 22, No. 10, 1984, pp. 1405–1412.

[14]Wilbur, P. J., "Advanced Ion Thruster Research," Tech. Rep. CR-168340, NASA, 1984.

[15]Albertoni, R., *Cathode Processes in MPD Thrusters*, Ph. d., Universita Degli Studi di Pisa, 2012.

[16]Katz, I., Anderson, J. R., Polk, J. E., and Brophy, J. R., "One-Dimensional Hollow Cathode Model," *Journal of Propulsion and Power*, Vol. 19, No. 4, 2003, pp. 595–600.

[17]Mikellides, I. G., Katz, I., Goebel, D. M., Polk, J. E., and Jameson, K. K., "Plasma processes inside dispenser hollow cathodes," *Physics of Plasmas*, Vol. 13, 2006.

[18]Wordingham, C. J., et al., "A Critical Review of Orificed Hollow Cathode Modeling: 0-D Models," *53rd AIAA/ASME/SAE/ASEE Joint Propulsion Conference & Exhibit*, 2017, AIAA-2017-4888.

[19]Miller, J. S., Pullins, S. H., Levandier, D. J., Chiu, Y. H., and Dressler, R. A., "Xenon charge exchange cross sections for electrostatic thruster models," *Journal of Applied Physics*, Vol. 91, No. 3, 2002, pp. 984–991.

[20]Hause, M., Prince, B., and Bemish, R., "Krypton charge exchange cross section for Hall effect thruster models," *Journal of Applied Physics*, Vol. 113, 2013.

[21]Lieberman, M. A. and Lichtenberg, A. J., *Principles of Plasma Discharges and Materials Processing*, Wiley Interscience, 2005.

[22]Hobbs, G. D. and Wesson, J. A., "Heat flow through a Langmuir sheath in the presence of electron emission," *Plasma Physics*, Vol. 9, No. 1, 1967, pp. 85–87.

[23]Domonkos, M. T., *Evaluation of low-current orificed hollow cathodes*, Ph.d., University of Michigan, 1999.

[24]Mandell, M. J. and Katz, I., "Theory of Hollow Cathode Operation in Spot and Plume Modes," *30th AIAA/ASME/SAE/ASEE Joint Propulsion Conference & Exhibit*, 1994.

[25]Hayashi, M., "Bibliography of Electron and Photon Cross Sections with Atoms and Molecules Published in the 20th Century - Xenon," Tech. Rep. NIFS-DATA-79, NIFS, 2003.

[26]Jones, E., Oliphant, T., Peterson, P., et al., "SciPy: Open source scientific tools for Python," 2001–, Online.

[27]Jameson, K. K., Goebel, D. M., and Watkins, R. M., "Hollow Cathode and Keeper-Region Plasma Measurements," *41st AIAA/ASME/SAE/ASEE Joint Propulsion Conference & Exhibit*, 2005.

[28]Katz, I., Anderson, J., Polk, J., and Brophy, J., "A Model of Hollow Cathode Plasma Chemistry," *38th AIAA/ASME/SAE/ASEE Joint Propulsion Conference & Exhibit*, 2002.

[29]Mikellides, I. G., Katz, I., Goebel, D. M., and Polk, J. E., "Hollow cathode theory and experiment. II. A two-dimensional theoretical model of the emitter region," *Journal of Applied Physics*, Vol. 98, No. 2005, 2005.

[30]Katz, I., Polk, J. E., Mikellides, I. G., Goebel, D. M., and Hornbeck, S. E., "Combined Plasma and Thermal Hollow Cathode Insert Model," *29th International Electric Propulsion Conference*, 2005.